Commensal-Related Changes in the Epidermal Barrier Function Lead to Alterations in the Benzo[a]Pyrene Metabolite Profile and Its Distribution in 3D Skin

Lisa Lemoine,[a,b] Dilan Bayrambey,[c] Alexander Roloff,[c] Christoph Hutzler,[c] Andreas Luch,[b,c] Tewes Tralau[a]

[a]German Federal Institute for Risk Assessment, Department of Pesticides Safety, Berlin, Germany
[b]Institute of Pharmacy, Department of Biology, Chemistry, Pharmacy, Freie Universität Berlin, Berlin, Germany
[c]German Federal Institute for Risk Assessment, Department of Chemical & Product Safety, Berlin, Germany

ABSTRACT Polycyclic aromatic hydrocarbons (PAH) such as benzo[a]pyrene (B[a]P) are among the most abundant environmental pollutants, resulting in continuous exposure of human skin and its microbiota. However, effects of the latter on B[a]P toxicity, absorption, metabolism, and distribution in humans remain unclear. Here, we demonstrate that the skin microbiota does metabolize B[a]P on and in human skin *in situ,* using a recently developed commensal skin model. In this model, microbial metabolism leads to high concentrations of known microbial B[a]P metabolites on the surface as well as in the epidermal layers. In contrast to what was observed for uncolonized skin, B[a]P and its metabolites were subject to altered rates of skin penetration and diffusion, resulting in up to 58% reduction of metabolites recovered from basal culture medium. The results indicate the reason for this altered behavior to be a microbially induced strengthening of the epidermal barrier. Concomitantly, colonized models showed decreased formation and penetration of the ultimate carcinogen B[a]P-7,8-dihydrodiol-9,10-epoxide (BPDE), leading, in consequence, to fewer BPDE-DNA adducts being formed. Befittingly, transcript and expression levels of key proteins for repairing environmentally induced DNA damage such as xeroderma pigmentosum complementation group C (XPC) were also found to be reduced in the commensal models, as was expression of B[a]P-associated cytochrome P450-dependent monooxygenases (CYPs). The results show that the microbiome can have significant effects on the toxicology of external chemical impacts. The respective effects rely on a complex interplay between microbial and host metabolism and microbe-host interactions, all of which cannot be adequately assessed using single-system studies.

IMPORTANCE Exposure to xenobiotics has repeatedly been associated with adverse health effects. While the majority of reported cases relate to direct substance effects, there is increasing evidence that microbiome-dependent metabolism of xenobiotic substances likewise has direct adverse effects on the host. This can be due to microbial biotransformation of compounds, interaction between the microbiota and the host's endogenous detoxification enzymes, or altered xenobiotic bioavailability. However, there are hardly any studies addressing the complex interplay of such interactions *in situ* and less so in human test systems. Using a recently developed microbially competent three-dimensional (3D) skin model, we show here for the first time how commensal influence on skin physiology and gene transcription paradoxically modulates PAH toxicity.

KEYWORDS coculture, skin model, commensals, benzo[a]pyrene, metabolites, skin barrier, GC-MS, BPDE DNA adducts, epidermal barrier

The skin is one of our largest organs and, as a physical and metabolic barrier, is our front line of defense against environmental impacts, physical as well as chemical (1). Moreover, it harbors a unique ecosystem of 10 to 100 trillion bacteria, fungi and

viruses, which together make up the skin microbiota (2–4). As a community with a complex interplay, this microbiota relies to a large extent on the few nutrients it can obtain from the stratum corneum (SC) as well as sebaceous, eccrine, and apocrine secretions (5). However, with the skin being a chronically nutrient-poor environment, the microbial commensals have to rely on the use of external carbon and energy sources in the form of xenobiotics (6, 7). Given the preferred growth of commensals in and on the SC, major xenobiotic sources of additional nutrients comprise reoccurring environmental exposures, from airborne pollutants to cosmetic ingredients or topically applied pharmaceuticals (8).

There is abundant evidence that the human microbiome can modulate exposure-response relationships of xenobiotic chemicals through some general mechanisms that could directly or indirectly affect toxicity (9). Respective mechanisms include direct metabolic conversions as well as indirect transformations. The latter include deconjugation of host-generated metabolites, modulation of epithelial barrier permeability, and regulation or alteration of endogenous host metabolism (9–14).

Among the most widespread environmental xenobiotics are polycyclic aromatic hydrocarbons (PAHs). Their ubiquitous occurrence leads to constant human exposure at low to medium levels (15, 16). Of particular toxicological interest are the potentially carcinogenic, high-molecular-weight representatives such as benzo[a]pyrene (B[a]P) (17, 18). With regard to the latter, it is actually the oxidative metabolic activation by cytochrome P450-dependent monooxygenases (CYPs) during human phase I metabolism that can trigger the formation of some of the most potent genotoxic carcinogens (19). For the metabolic activation of B[a]P, two of the most important enzymes involved in the formation of the ultimately reactive species are CYP1A1 and CYP1B1 (20). The resulting electrophilic metabolite B[a]P-7,8-dihydrodiol-9,10-epoxide (BPDE) is prone to DNA adduct formation, preferentially at nucleophilic guanine residues, leading to the formation of dG-N2-BPDE (21). While the formation of the biologically dysfunctional dG-N2-BPDE makes BPDE a strong genotoxin, overall toxicity will strongly depend on any phase I and phase II detoxification preceding actual adduct formation as well as on the rate of DNA repair (22). It should be noted, however, that before being subject to host metabolism, PAHs obviously first need to pass the epidermis, which is a highly functional physicochemical barrier (23).

Exposure to PAHs predominantly occurs first on the skin with human commensal microbes hence being the first point of (metabolic) contact (24, 25). Previous studies from our lab have shown a ubiquitous potential of the commensal microbiome for B[a]P-degradation. Some of the bacterial genes for the respective underlying metabolic pathways were identified and shown to be detectable *in situ* on human skin, as were the associated bacteria. Concomitantly carbon-limited batch cultures showed the corresponding bacterial metabolism of B[a]P to result in the formation and excretion of highly cytotoxic and genotoxic metabolites (26, 27). Similar observations have been reported for the intestinal microbiota, where commensals are known to directly metabolize xenobiotic substances, as well as impacting the host's capacity for xenobiotic metabolism by affecting phase I and phase II enzymes (28–30).

While these studies deliver valuable insights into the various aspects of how commensal metabolism of xenobiotics can influence host toxicity, they fall short of addressing the complex and faceted interplay systemically. The reason for this is commensal species specificity together with a lack of suitable model systems. We therefore recently reported the development of a new commensal 3D skin model (31). We have now applied this model to investigate commensal B[a]P-metabolism and its potential toxicologically relevant effects *in situ*. These results provide insights into the complex interplay between microbially induced xenobiotic metabolism of B[a]P as a procarcinogen and the host organ skin under near *in vivo* conditions (see Data Set S1 for experimental setup). The data indicate a complex pattern of host-microbe interactions that were not accessible in previous single-system studies.

RESULTS

The aim of the study was to investigate the effects of commensal skin colonization on B[*a*]P-metabolism *in situ* using a microbially competent 3D skin model (31). The model was colonized with two previously isolated skin commensals, namely, *Micrococcus luteus* 1B and *Pseudomonas oleovorans* 1C (26, 27). While both organisms have been established using B[*a*]P as the sole source of carbon and energy, including the metabolites formed by *M. luteus*, the nature of the metabolites formed by *P. oleovorans* remained unknown (27). We therefore started with a comprehensive characterization of B[*a*]P metabolites formed by the latter using carbon-limited batch cultures.

P. oleovorans B[*a*]P metabolites. The analytical examination of the respective culture supernatants confirmed this strain's ability to partially metabolize B[*a*]P (26). The dominant metabolites formed were B[*a*]P-1,6-dione, B[*a*]P-7,8-dione, B[*a*]P-7,10-dione, and 3-OH-B[*a*]P (Fig. S4A). Altogether, a total of 8 metabolites could be identified, 3 of which seem to be specific for this particular organism (Fig. S4B and C). Among them were 8-OH-B[*a*]P, B[*a*]P-7,10-dione, and an additional monohydroxylated B[*a*]P, which could not be further specified (Fig. S4D).

Analytical characterization of commensal B[*a*]P metabolism *in situ* and effect on BPDE-DNA adduct formation. With the PAH metabolite patterns of both microorganisms established, it was possible to follow B[*a*]P metabolism and distribution of resulting metabolites in the colonized skin model. For this purpose, B[*a*]P was topically applied to stably established microbial competent 3D skin cultures for 7 days. Following substance treatment, the concentration of B[*a*]P and its metabolites was measured starting from the surface throughout the model on day 8, with analyte levels in the supporting culture medium being monitored over the entire cultivation period (Data Set S1).

The data indicate that commensal B[*a*]P metabolism occurs directly at the surface with the cocolonized models, which also retained larger amounts (2 of 3 were significantly higher) of unmetabolized B[*a*]P than uncolonized 3D skin (Fig. S5A). Furthermore, the concentrations of all detected B[*a*]P-diones as well as 3-OH-B[*a*]P were strongly elevated, all of which were established metabolites of at least one of the two commensals. B[*a*]P-7,10-dione was formed only in the presence of *P. oleovorans* (Fig. S5B). Notably, concentrations of the eukaryotic B[*a*]P-7,8,9,10-tetrahydrotetrol (B[*a*]P-tetrol; i.e., the hydrolysis product resulting from *trans*-opening of the epoxide moiety in BPDE) were slightly elevated in the presence of *M. luteus* (Fig. 1A).

Except for B[*a*]P-7,10-dione, all of the above-mentioned metabolites were also detectable in the epidermis and dermis. The predominant species were B[*a*]P-1,6-dione, B[*a*]P-6,12-dione, and B[*a*]P-7,8-dione or just B[*a*]P-7,8-dione, respectively (Fig. 1B and C). For all monitored metabolites, there was a clear colonization-dependent impact, indicating a distinct microbiome-mediated effect (Fig. S6A to C). In addition, the epidermis of models cocolonized with both organisms tended to contain lower concentrations of B[*a*]P-diones than the surface. In the deeper dermal layers, this effect was less pronounced.

Notably, commensal colonization led to significantly reduced levels of B[*a*]P-9,10-diol and B[*a*]P-tetrol in all investigated epidermal and dermal samples (Fig. S6D and E). Also, the concentration of unmetabolized B[*a*]P was greatly reduced in the dermis of commensal models, with the strongest effect occurring in the mixed coculture (Fig. 1B and C; Fig. S6C).

Several of the metabolites passed through the entire model and were detectable in the basal cell culture medium. These were B[*a*]P-tetrol, B[*a*]P-9,10-diol, B[*a*]P-7,8-diol, 3-OH-B[*a*]P, B[*a*]P-1,6-dione, and B[*a*]P-6,12-dione, which initially appeared 24 h after the first application of B[*a*]P to the model surface, and 7-OH-B[*a*]P, which appeared after 48 h (Table S1A). The corresponding concentrations increased in a time-dependent manner until reaching a plateau phase from day 5 onward, with the samples of the colonized models featuring significantly lower levels of B[*a*]P and B[*a*]P metabolites (Fig. S6F). This effect was particularly pronounced with *M. luteus*.

In concordance with this and with what was found for B[*a*]P-9,10-diol and B[*a*]P-tetrol (that is, the significant reduction of metabolite levels in the microbe-colonized models), BPDE-DNA adducts were also found to be strongly reduced in models
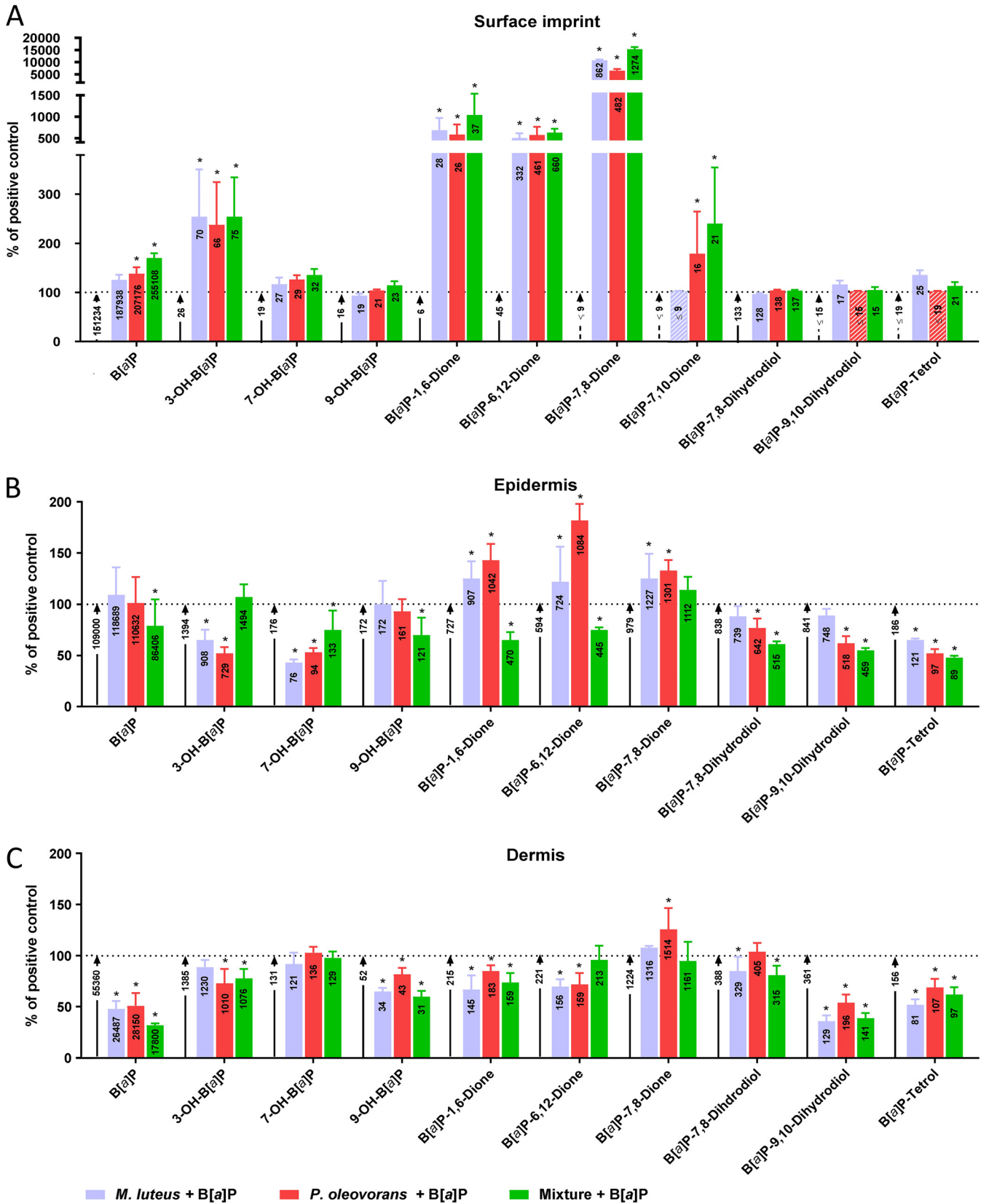
FIG 1 Concentrations of B[*a*]P and its metabolites from the surface imprint (A), epidermis (B), and dermis (C) of microbial skin tissue coculture colonized as indicated after 7 days of repeated B[*a*]P treatment, as determined via GC-MS. Each bar represents 6 biological replicates (mean + SD) relative to the B[*a*]P-treated uncolonized control. Each bar depicts the measured substance concentrations in pmol/skin model. The concentration of the B[*a*]P-treated control

(Continued on next page)
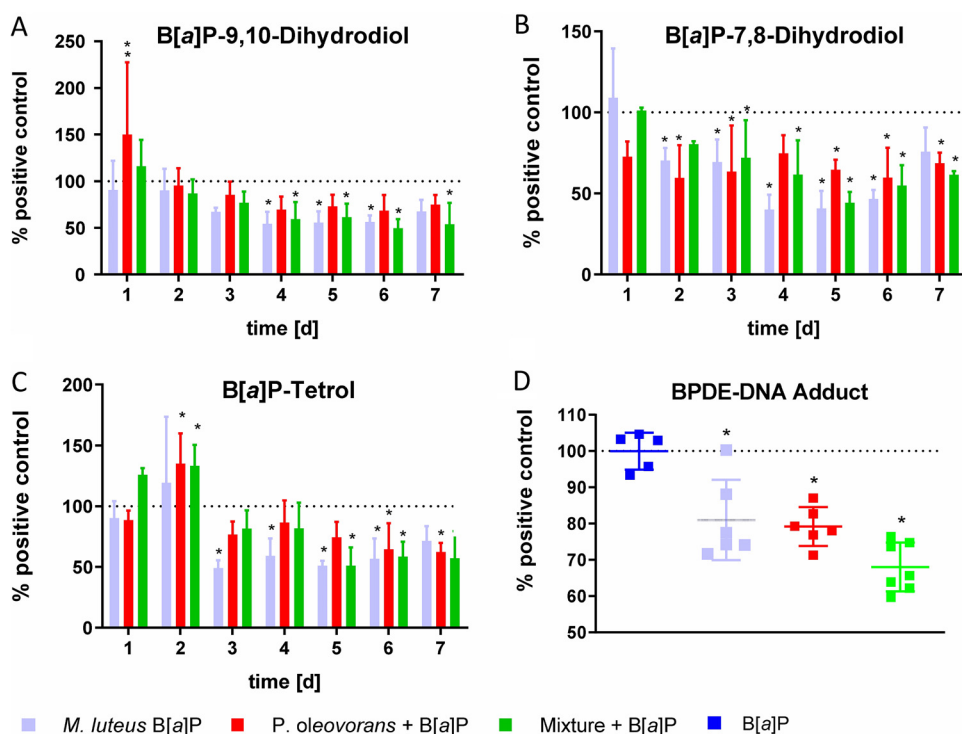
FIG 2 Concentrations of 3 representative B[*a*]P metabolites in the basal culture medium of microbial skin tissue cocultures over 7 days of repeated B[*a*]P treatment, as determined via GC-MS. Each bar represents 6 biological replicates. (A) B[*a*]P-7,8-dihydrodiol, (B) B[*a*]P-9,10-dihydrodiol, and (C) B[*a*]P-tetrol levels (mean + SD) as percentages of the B[*a*]P-treated uncolonized control. (D) Number of BPDE-DNA adducts of the microbial skin tissue cocultures colonized as indicated, compared to the B[*a*]P-treated control lacking a microbiota. Epidermis and dermis were examined as a whole. The observed differences are considered significant (*, $P < 0.05$).

subjected to commensal colonization (Fig. 2). Meanwhile, controls without B[*a*]P showed no BPDE-DNA formation, irrespective of their microbial competence.

Commensal impact on skin function. The potential functional impact of commensal B[*a*]P-metabolism on the host and skin function was studied using transcriptomic assays. The Clariom S system records the activity of more than 20,000 well-annotated transcripts, hence providing coverage of most of the functionally annotated genes. Compared to uncolonized controls, treatment of colonized models with B[*a*]P significantly affected more than 2,500 transcripts, while substance treatment alone had an effect on 1,300 transcripts (Fig. S7). Comparison among all treatment groups showed that 10 of the 17 most influenced transcripts strikingly encode proteins that play a role in epidermal differentiation, all of which were repressed in cocolonized models as well as after treatment with B[*a*]P (Fig. 3). This includes several epidermal differentiation complex (EDC) genes, such as those encoding filaggrin (FLG), loricrin, and caspase 14.

The results of the transcriptome analysis strongly imply a potential commensal influence on skin differentiation, particularly following substance treatment. Subsequent analysis therefore focused on the fluorescent visualization of various functional markers for different stages of differentiation as well as a tight junction (TJ) marker (Fig. 4A and Fig. S8). In the B[*a*]P-exposed models, bacterial colonization led to a strong increase in the late differentiation markers FLG and involucrin (IVL), with a particularly strong increase for *P. oleovorans* and mixed skin tissue (Fig. 4A and B).

FIG 1 Legend (Continued)

lacking a microbiota is indicated in the arrow next to the respective bar. For substances that could not be measured, the concentration is indicated as being below the smallest measured concentration in calibration, and corresponding columns or arrows are hatched. The observed differences are considered significant (*, $P < 0.05$).
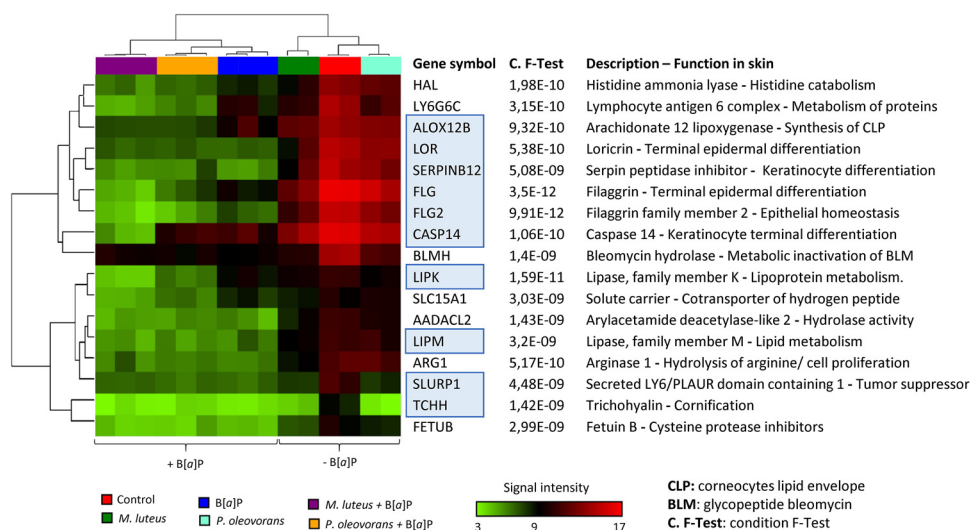
FIG 3 Hierarchical clustering of the 17 most significantly regulated genes according to the conditions of the F test in microbial skin tissue coculture with and without B[a]P treatment. Shown are the signal intensities of the transcripts measured using Clariom S microarray analysis. Ten of these 17 genes code for proteins that are related to epidermal differentiation and are marked in blue. In addition, a description and the most likely function in the skin are presented for each gene listed.

In light of the skin's dual function as a physicochemical barrier, we further investigated the commensal impact on the expression of several key proteins involved in human B[a]P metabolism. Enzymatic expression of CYP1A1 was found to be decreased in the commensal models following treatment with B[a]P, while there was no clear effect on CYPs 1B1 and 1A2 or epoxide hydrolase 1. In contrast, both microorganisms led to increased expression of the regulatory cofactor aryl hydrocarbon receptor nuclear translocator (ARNT), even in the absence of B[a]P (Fig. 5A and B).

Metabolic activation of B[a]P in eukaryotes can lead to the formation of bulky DNA adducts that can be repaired by the nucleotide excision repair pathway (NER). The treatment of 3D skin models with B[a]P resulted in an increase in the expression of xeroderma pigmentosum complementation group C (XPC) and XPG proteins, both of which are typical representatives of this repair pathway (Fig. 6B). Following B[a]P treatment, however, their gene and protein expression was significantly reduced in microbe-colonized skin tissue compared to the control treated with B[a]P only (Fig. 6A and B).

DISCUSSION

Growing evidence suggests potential chemical-associated effects of microbiome-host interactions on human health (7, 32, 33). However, toxicity studies are still largely conducted without particular consideration of the microbiota (34). At best, the microbiota is considered a systemic compartment when toxicity is tested *in vivo*. However, this does not consider the high species specificity of microbiota, nor does it acknowledge that even without this species specificity the microbiotas of laboratory animals are strongly impacted by the artificial environments the animals are housed in and thus are hardly representative (31). In the context of risk assessment of xenobiotic exposure, this not only is scientifically unsatisfying but also carries a true risk of missing relevant health effects. However, apart from a partial lack of awareness of this issue, another major point has been a lack of appropriate models to systematically study such effects. This is true for the gut but also for the skin (7, 35). For dermal environments the recent development of our microbially competent coculture model partly overcomes this, as it makes it possible to study microbially driven modulation of B[a]P metabolism and toxicity and its effects on the host (31). The results confirm that the previously observed commensal metabolism of B[a]P also occurs *in situ* (26, 27). However, and more importantly, they provide a first glance at the corresponding
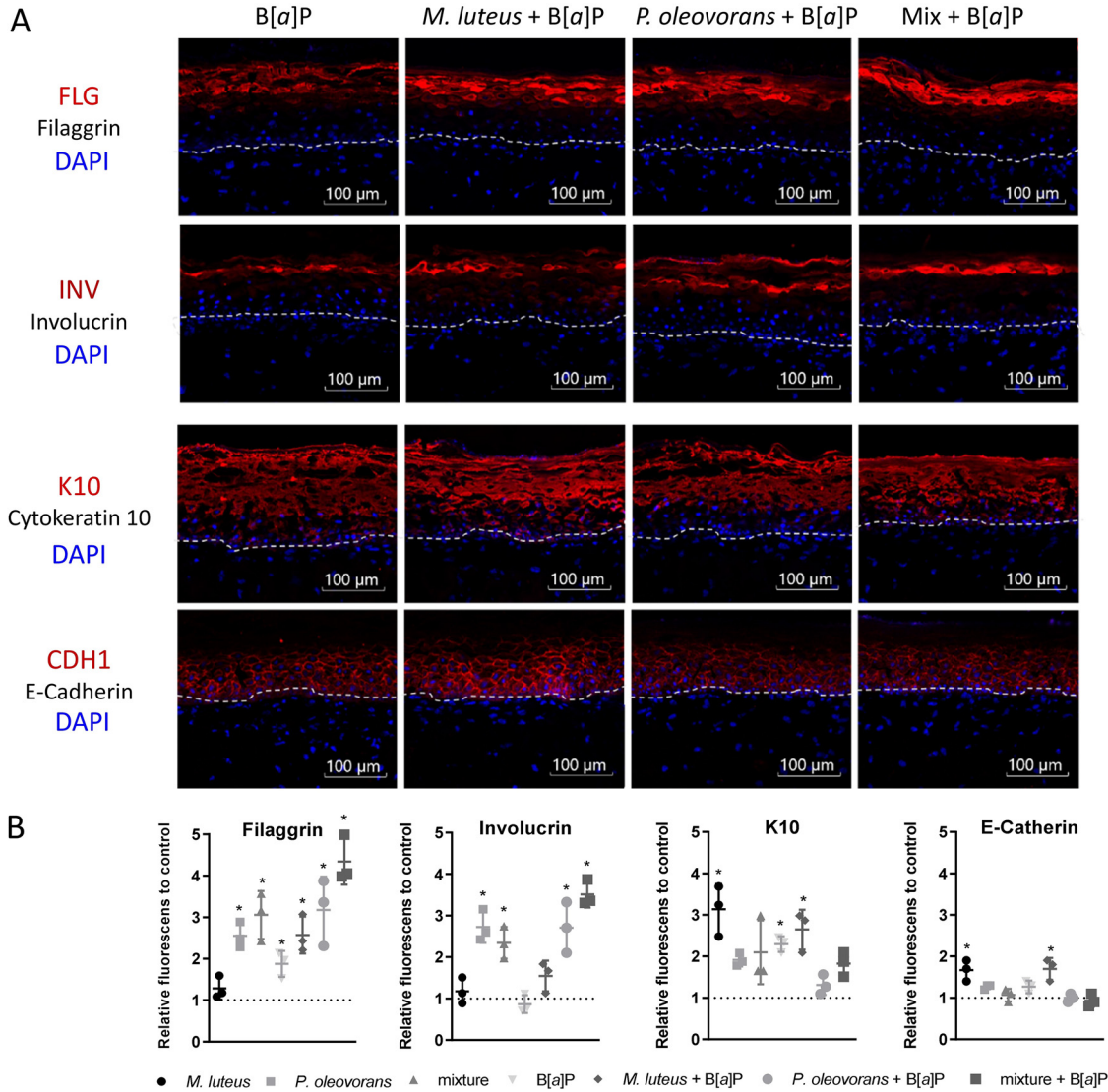
FIG 4 Expression of epidermal differentiation markers in microbial skin tissue cocultures with and without B[a]P treatment. (A) Immunostaining of selected differentiation markers and a tight junction marker of skin sections of microbial competent skin models, colonized as indicated and with B[a]P treatment. All antibody stains are red, and the cell nuclei stained blue with DAPI. The dashed line indicates the course of the basal lamina. (B) Summary of the immunostaining of 3 biological replicates relative to the uncolonized skin, including all controls without B[a]P application. The observed differences are considered significant (*, $P < 0.05$).

metabolite patterns along skin layers and how this potentially affects host toxicity in a complex and hitherto unexpected manner.

Skin colonization leads to an accumulation of unmetabolized B[a]P and bacterial metabolites, including B[a]P-1,6-dione, B[a]P-6,12-dione, B[a]P-7,8-dione, B[a]P-7,10-dione, and 3-OH-B[a]P (27), on the skin surface and, partially, in the epidermis. The strong increase of these commensal metabolites points to microbiotic recruitment of B[a]P as a source of carbon and energy and is in line with previous *in vitro* studies (26, 36). This is particularly evident in the case of B[a]P-7,10-dione, which, being a metabolite of *P. oleovorans*, occurred exclusively on the surface of the correspondingly colonized skin models. However, the identification of B[a]P-tetrol and B[a]P-9,10-dihydrodiol on the surface of skin harboring *M. luteus* shows that concomitant human phase I metabolism occurs, as neither of the two metabolites occurred in bacterial batch cultures (27). Notably, when assessed throughout their various compartments, the colonized models showed a slight overall decrease of B[a]P metabolites compared
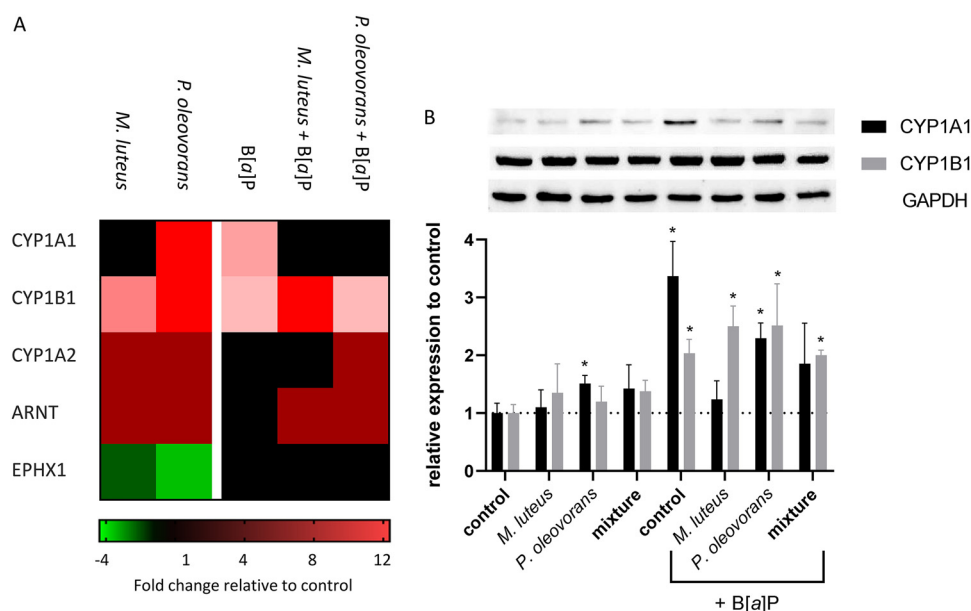
FIG 5 Expression of enzymes involved in B[a]P activation in microbial skin tissue coculture. (A) Cluster map showing the fold change compared to uncolonized skin at day 8 of microbial colonization. Shown are the gene symbols of significantly differentially expressed genes with a P value of ≤0.05. (B) Immunoblot of total protein of microbial skin tissue coculture, colonized as indicated, as well as the summary of the immunoblots of 3 biological replicates relative to the uncolonized skin. The observed differences are considered significant (*, $P < 0.05$).

to uncolonized skin (~4.5%), which was significant for a majority of the metabolites. This included B[a]P-tetrol, where the respective strong reduction consequently points to fewer BPDE-DNA adducts being formed beforehand, an effect most pronounced in the presence of *P. oleovorans* and its mixed coculture. Likewise, the expression of key enzymes of the NER (XPC and XPG) was reduced in microbial skin tissue cocultures. In
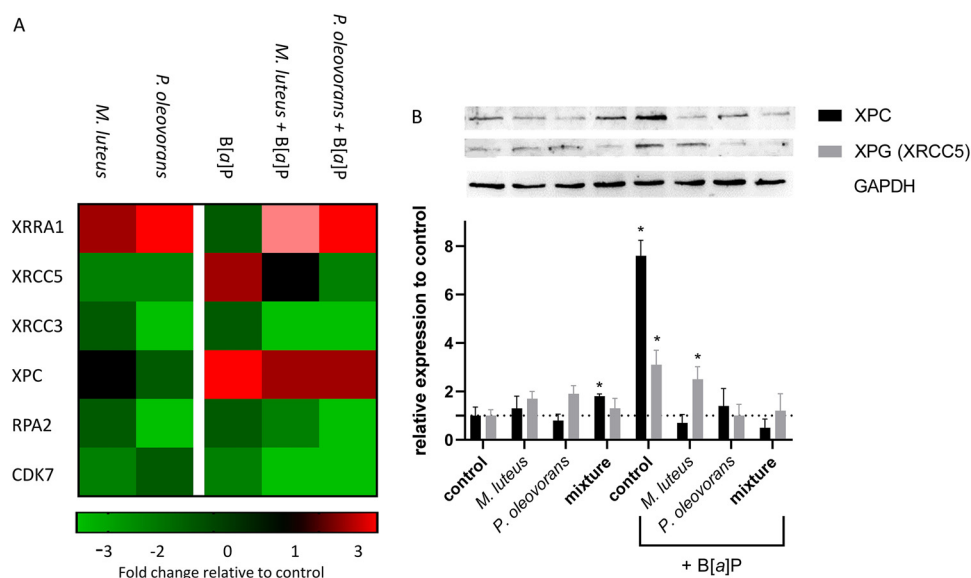
FIG 6 Expression of enzymes of the nucleotide excision repair (NER) pathway in microbial skin tissue coculture. (A) Cluster map showing the fold change compared to uncolonized skin at day 8 of microbial colonization. Shown are the gene symbols of significantly differentially expressed genes with a P value of <0.05. (B) Immunoblot of total protein of microbial skin tissue coculture, colonized as indicated, as well as the summary of the immunoblots of 3 biological replicates relative to the uncolonized skin control. The observed differences are considered significant (*, $P < 0.05$).

addition, the amount of B[*a*]P-tetrol as well as other metabolites passing through the model into the basal medium was significantly reduced in the commensal models, with *M. luteus* leading to nearly 50% reduction. This indicative beneficiary commensal effect is in contrast to what was observed previously with batch cultures, where bacterial metabolism of B[*a*]P actually enhanced B[*a*]P-mediated genotoxicity (27). Given that the colonized models show production of the same metabolites *in situ*, the effect observed here came as a surprise.

Together, the results therefore strongly point to commensally induced changes in skin metabolism and/or barrier function. Overall, the analytical results of the uncolonized skin models match those of a previous study by Brinkmann et al. (37), who showed that MatTek's EpiDermFT metabolizes B[*a*]P to form typical human metabolites. However, in the uncolonized models, only a small fraction of B[*a*]P is metabolized due to the low or absent metabolic activity of corneocytes. Only about 5.2% of the applied B[*a*]P was metabolized, with the remaining B[*a*]P accumulating on the skin surface and in the epidermis (Table S1B). Since lipophilic compounds steadily penetrate the skin by passive diffusion, this induces the buildup of a substance reservoir (38). Befittingly, for the uncolonized models, the major amount of the B[*a*]P was indeed found to be metabolized in the metabolically active epidermis. In agreement with the work of Bourgart et al. (39), the more hydrophilic metabolites, such as B[*a*]P-tetrol, B[*a*]P-7,8-diol, and B[*a*]P-9,10-diol, subsequently penetrated throughout the skin, while B[*a*]P predominantly remained in the upper layers (39). Meanwhile, the colonized models are also metabolically active but feature increased accumulation of B[*a*]P and known bacterial metabolites on the surface as well as showing an altered layer-specific decrease. On the transcriptomic level, this was accompanied by strong changes in key transcripts involved in epidermal differentiation.

The general observation of commensals influencing skin differentiation matches previous results from other studies, including animals (40). The most strongly altered transcripts include LIPM and LIPK, both of which have an essential function in lipid metabolism of the most differentiated epidermal layers (41). Another heavily affected transcript is CASP14, which is a predominant caspase in the epidermal SC and is required for cornification (42). The reduced transcript levels are in line with the age of the models at the time of sampling. Instead, selected corresponding protein markers of skin differentiation were revealed to be elevated. Such an apparent commensal-related strengthening of the skin barrier has indeed been observed before, although not in a toxicological context and without such a strong modulatory effect on systemic substance metabolism and availability (43, 44). Our results show that *P. oleovorans* had a particularly strong influence, promoting terminal differentiation as exemplified by an increase in the expression of FLG and IVL. In contrast, colonization with *M. luteus* leads to less pronounced changes, showing a slight but significant enhancing effect on FLG, K10, and the TJ marker E-cadherin. Simultaneous colonization of the 3D skin models with both organisms revealed the greatest increases in expression of IVL and FLG, supporting the finding of Loomis et al. (44) that FLG expression is more strongly enhanced by multiple commensals than by a single species. The large amount of unmetabolized B[*a*]P on the surface of the mixed microbial skin tissue cocultures suggests that FLG and IVL particularly contribute to a reduction in the diffusion of chemicals into the skin. This is in agreement with the results of Joensen et al. (45), who showed that loss-of-function mutations of FLG lead to increased internal exposure to phthalate metabolites. IVL is also important for skin permeability to chemicals, with a triple knockout of IVL, envoplakin, and periplakin resulting in a defective epidermal barrier (46). Moreover, tissue permeability is regulated by TJs and keratin filaments (47), whose expression can be enhanced by the presence of commensal and probiotic strains (48). In our models, *M. luteus* particularly induced E-cadherin and K10. It seems reasonable to assume that the resulting strengthening of the epidermis is causative of the respective strong effects on metabolite concentrations in the dermis and basal cell culture medium, respectively. At the same time, commensally induced increased terminal

differentiation of the SC (i.e., as seen for *P. oleovorans*) promotes the accumulation of B[*a*]P on the skin surface, thus reducing the rate of epidermal skin-type B[*a*]P metabolism. As this strongly affects levels of B[*a*]P-9,10-diol, B[*a*]P -7,8-diol, and BPDE, it would obviously reduce the number of BPDE-DNA adducts in general.

The altered barrier function also systemically affected key genes of human phase I metabolism. Effects were seen particularly for the AhR signaling pathway, namely, ARNT, CYP1B1, and CYP1A1, with the effect being particularly strong on the latter. Although CYP1A1 expression is increased in coculture with *P. oleovorans*, it is significantly reduced after repeated B[*a*]P application in all studied microbial cocultures compared to uncolonized skin. This is likely attributed to the smaller amount of B[*a*]P penetrating the SC, which in turn reduces the available concentration in the metabolically active part of the epidermis. In the context of B[*a*]P toxification, the commensal influence on the skin barrier hence apparently outweighs any microbially induced changes in CYP expression. Our results clearly show that commensals are able to metabolize as well as potentially toxify B[*a*]P on and in human skin. However, with regard to B[*a*]P genotoxicity, the microbial effects on host skin differentiation have a strong modulating beneficial influence due to an enhanced physicochemical barrier function. The latter alterations cause a commensal-related reduction of the toxicity of B[*a*]P especially by inhibiting the uptake of this procarcinogen and its subsequent metabolic activation. The microbial influence on epithelial permeability and integrity has important implications for the absorption, metabolism, and distribution of xenobiotics and environmental pollutants such as B[*a*]P. Overall the results demonstrate the respective microbe-host interactions to have much more complex effects on substance toxification and metabolism than previously inferred from studies on single systems. Depending on the particular substance and circumstances, this could lead to either over- or underestimation of toxicity, both of which should be avoided. Therefore, there is an urgent need to address the effect of the microbiome on potential systemic host toxicity more systematically. Given the species specificity of the microbiome, this has to be implemented using commensally competent testing systems that are specific for the human host.

MATERIALS AND METHODS

Skin models obtained from MatTek rely on ethically sourced materials from accredited institutes and are subject to strict donor consent. Their suppliers have represented in writing that they are strictly regulated by and comply with U.S. federal government standards.

Chemicals and media. Gas chromatography-mass spectrometry (GC-MS)-grade solvents were purchased from Thermo Fisher Scientific (Waltham, MA, USA). All other chemicals were sourced from Sigma-Aldrich (St. Louis, MO, USA) unless otherwise noted. EpiDermFT tissue models with lot numbers 29346, 25358, 25392, 29308, and 29388 and associated maintenance medium were from MatTek (Ashland, MA, USA). Analytical standards were purchased from MRIGlobal Chemical Carcinogen Repository (Kansas City, MO, USA): B[*a*]P, 7-OH-B[*a*]P, 9-OH-B[*a*]P, B[*a*]P-*trans*-7,8-dihydrodiol(±), B[*a*]P-*trans*-9,10-dihydrodiol(±), B[*a*]P-1,6-dione, B[*a*]P-6,12-dione, B[*a*]P-7,8-dione, B[*a*]P-*r*-7,*t*-8,*t*-9,*c*-10-tetrahydrotetrol, benzo[*a*]anthracene-*cis*-5,6-dihydrodiol (B[*a*]A-*cis*-5,6-dihydrodiol), 5-methylchrysene-*r*-1,*t*-2,3,*c*-4-tetrahydrotetrol, and deuterated B[*a*]P-D$_{12}$. 3-OH-B[*a*]P, 3-OH-B[*a*]P-^{13}C$_6$, and B[*a*]P-1,6-dione were from Toronto Research Chemicals (North York, ON, Canada).

Bacterial isolates and bacterial growth. Cocultures were set up as previously described, with 10^4 to 10^6 cells of *Micrococcus luteus* 1B and/or *Pseudomonas oleovorans* 1C used for skin inoculation (31).

Beforehand, to determine the B[*a*]P metabolites of *P. oleovorans*, the latter was cultured in minimal medium (MM) supplemented with 100 μM B[*a*]P as previously described for *M. luteus* by Sowada et al. (27). Cell harvesting was performed daily over a period of 2 weeks. For later analytical examination, 25 ml of the bacterial culture supernatant was frozen and stored at $-20°C$.

Tissue viability assay for selection of the applied B[*a*]P concentration. As the basis for our coculture, we used the full-thickness skin model EpiDermFT from MatTek (Ashland, MA, USA). Directly after delivery, the models were transferred into six-well plates (Greiner Bio-One, Frickenhausen, Germany) with 2.5 ml of antibiotic-free EPI-100-MM-ABF maintenance medium and cultivated for 24 h to recover at 37°C and 5% CO$_2$ as recommended by the manufacturer. Before treatment of the actual microbial skin tissue coculture with B[*a*]P, we first evaluated 3 different concentrations of B[*a*]P (5 nM/cm^2, 50 nM/cm^2, and 500 nM/cm^2) and determined their influence on tissue viability via an MTT [3-(4,5-dimethyl-2-thiazolyl)-2,5-diphenyl-2H-tetrazolium bromide] assay. A high B[*a*]P concentration can promote bacterial use as a food source but could impair the viability of the skin cells and thus inhibit its B[*a*]P metabolism. The MTT assay was performed using MatTek's MTT concentrate, MTT diluent, and MTT extractant according to the manufacturer's instructions. The skin models (1-cm^2 diameter) were treated daily with one of the 3 B[*a*]P concentrations prepared in acetone of analytical grade or solvent control (pure acetone),

respectively. Acetone was chosen as the deposition vehicle due to its successful use in other skin B[a]P metabolism studies (37, 39, 49). The cell culture medium was exchanged daily, and the MTT assay was carried out after 3 and 7 days of B[a]P treatment. With moderate viability losses of 15% after 7 days of B[a]P application, the mean concentration of 50 nM/cm^2 was chosen for further experiments (Fig. S1).

Tissue culture and bacterial quantification. The EpiDermFT models were routinely cultivated and subjected to bacterial inoculation or solvent treatment as described earlier (31). Bacterial inoculation of the respective models was performed using three droplets of bacterial suspension at a volume of 5 μl each, with the droplets evenly spaced across the model surface and then left to dry. At 24 h after establishing the coculture of the B[a]P-degrading skin commensals, 50 nM/cm^2 B[a]P was applied as evenly as possible on the surface of the skin tissues (diameter, 1 cm^2). Identical amounts of solvent were applied in control experiments. This procedure was repeated daily at the same time during the cultivation period of 8 days, stopping 24 h before harvesting the EpiDermFT models. In total, each model was treated with B[a]P for 7 consecutive days, resulting in a total concentration of 350 nmol/skin model. Tissues and the daily collected basal cell culture medium were separately stored at −80°C until further processing.

Bacterial growth in coculture was quantified using plate counts, since there was no significant added value in using quantitative PCR (qPCR) additionally (31). As in our previous experiments, viable colony counts (CFU/cm^2) showed stable quantities for *M. luteus* from day 4 of cultivation (Fig. S2A and C), while those of *P. oleovorans* increased slightly and were on average slightly higher. As reported previously, *M. luteus* appeared to grow exclusively on the SC, while *P. oleovorans* also penetrated into the dermis, although to a small extent (approximately ≤10%) (31). The cell numbers shown in Fig. 2 refer to those on the skin surface. In general, the B[a]P application had no significant influence on cell numbers (Fig. S2C). The selection of *P. oleovorans* and *M. luteus* as models for commensal B[a]P degraders followed both biological and practical considerations (31). Briefly, the selection covers species of both Gram variants as well as two of the major phyla of the skin's microbiome. Both species are biologically relevant and have been repeatedly isolated from healthy subjects at different skin sites (26). Moreover, they are easily distinguishable from each other on agar plates and have a well-established potential for xenobiotic metabolism (26, 50).

Transcriptome analysis. In order to gain insight into microbial-related changes in the skin's gene expressions after B[a]P application, the skin tissues were examined as previously described by microarray analysis (31). For this purpose, total RNA was recovered subsequent to cell harvesting with a TissueLyser II (Qiagen, Hilden, Germany). The RNA was isolated with a TRIzol-based protocol using the TRIzol reagent (Thermo Scientific, Waltham, MA, USA) as described earlier (51). Microarray analysis was performed using duplicates of controls (uncolonized skin and *M. luteus*/*P. oleovorans* skin tissue coculture) and triplicates of treatments (B[a]P treatment and *M. luteus*/*P. oleovorans* with B[a]P application) in Clariom S human assays (Applied Biosystems, Foster City, CA, USA) at ATLAS Biolabs (Berlin, Germany). Data evaluation and interpretation were done using Transcriptome Analysis Console software v4.0.1.36 (TAC) (Applied Biosystems, Foster City, CA, USA) ($P \leq 0.05$).

Immunofluorescence. To investigate changes in the epidermal barrier function, we snap-froze the skin tissues on day 8 of the cultivation in Tissue-Tek O.C.T. compound (Sakura Finetek, Torrance, CA, USA) using liquid nitrogen and stored these at −80°C until use. Tissues were cut into 7-μm-thick sections at −20°C using a Microm HM 550 cryostat and mounted on Super-Frost slides (both from Thermo Fisher Scientific, Waltham, MA, USA). Subsequently, cryosections were fixed for 10 min with ice-cold methanol (−20°C). Antibody (Ab) staining was performed as described by Hering et al. (52). The following antibodies were used: rabbit Ab against cytokeratin 10 (18343-1-AP) and involucrin (55328-1-AP; Proteintech Group, Rosemont, IL, USA) and mouse Ab against filaggrin (NBP2-53245-20; Novus Biologicals, Littleton, CO, USA) and E-cadherin (33-4000; Thermo Scientific, Waltham, MA, USA) at a concentration of 5 μg/ml. The appropriate secondary antibodies conjugated to Alexa Fluor 594 (red) (Molecular Probes, Eugene, OR) were applied (1:400 in phosphate-buffered saline with 0.1% Tween [PBST]) followed by Hoechst 33258 (Sigma-Aldrich, St. Louis, MO, USA) (1 μg/ml in Dulbecco's phosphate-buffered solution [DPBS]) application for counterstaining the nuclei. Sections were embedded in mounting medium and analyzed in biological triplicates using the LSM700 confocal microscope (Carl Zeiss, Oberkochen, Germany).

Western blot analysis. To determine potential changes in protein levels, Western blot analysis of selected proteins was carried out. The proteins were isolated in 100 μl of a urea buffer (8 M, pH 8.5) combined with lysis using a TissueLyser II (Qiagen, Hilden, Germany) operated for 5 min at 20 Hz. The cell residues were separated by centrifugation at a relative centrifugal force (rcf) of 10,000 for 10 min. Total protein concentration was evaluated using a bicinchoninic acid (BCA) assay (Thermo Fisher Scientific, Darmstadt, Germany). In general, 20 μg of total protein was then subjected to SDS-PAGE and transferred to nitrocellulose membranes following standard protocols. Primary antibodies against CYP1A1 (ABIN1872160; Antibodies-online Inc., Limerick, PA, USA), CYP1B1 (ABIN3184162), XPC (ABIN2855495), XPG (ABIN3187504), and glyceraldehyde 3-phosphate dehydrogenase (GAPDH) (ABIN2666338) were used for subsequent immunostaining, followed by visualization with appropriate horseradish peroxidase-coupled secondary antibodies (Santa Cruz Biotechnology) and enhanced chemiluminescence (34078; Thermo Scientific, Waltham, MA, USA) for detection in the Fusion FX6 Edge system (Vilber Lourmat, Eberhardzell, Germany).

GC online-coupled to MS. (i) Analysis of *P. oleovorans* B[a]P metabolites. To assess the bacterial influence on the human B[a]P metabolism, knowledge of the identity of the corresponding microbial B[a]P degradation products is crucial. For this reason, we analyzed the B[a]P metabolism of *P. oleovorans* via GC-MS strictly following a previously described protocol applied to *M. luteus* (27). This applies to the extraction, sample preparation, and GC-MS analysis. The verification was done using retention time (RT) and mass spectra (MS) of authentic references.

TABLE 1 Internal standards[a]

Substance	RT (min)	Quantifier m/z	Qualifier m/z	Designation
B[a]P-D$_{12}$	26.6	264	262	1
3-OH-B[a]P-^{13}C$_6$	34.9	346	347	2
Chrysene 1,4-dione	29.0	404	405	3
B[a]A-cis-5,6-diol	22.7	406	316	4
5-Methylchrysene-1,2,3,4-tetrahydrotetrol	29.6	304	394	5

[a]Internal standards used for verification of B[a]P metabolite extraction and silylation. Designations correspond to the external standards listed in Table 2.

(ii) B[a]P metabolism in microbial skin tissue coculture. In order to determine the microbial influence on the B[a]P metabolite profile and distribution within the skin, the levels of B[a]P and its metabolites were quantified in surface imprint, tissue samples, and culture media from 6 biological replicates using GC-MS.

(a) Cell lysis. First, the surface imprint was taken as described earlier (31). The resulting cell pellet was digested by freeze-thawing. Three cycles of freezing cells in a dry ice-ethanol bath for 10 min and subsequent thawing at room temperature for 10 min were performed as described by de Bruin and Birnboim (53). For the subsequent metabolite extraction, the lysates were diluted with 750 μl PBS. The lysis of the skin tissues was done mechanically and enzymatically. Prior to cell lysis, the epidermis and dermis were separated, followed by homogenization with a TissueLyser II instrument twice for 5 min each at 20 Hz in 750 μl PBS each and digestion with 1 U/ml LiberaseTH enzymes (Roche, Mannheim, Germany) for 20 min at 37°C. The cell culture medium was used directly for metabolite extraction.

(b) Metabolite extraction. The surface imprint lysates, the skin tissue lysates, and the cell culture media (2.5 ml each) were spiked with a mixture of internal standards (Table 1) at a final concentration of 500 ng/ml (internal standard [IS] 2 = 1.8 μM, IS 3 = 1.9 μM, IS 4 = 1.9 μM, and IS 5 = 1.6 μM) in dimethyl sulfoxide (DMSO), except for B[a]P-D$_{12}$, which was at 50 μg/ml (IS 1 = 181.1 μM) in DMSO (Table 1). The latter is due to the high B[a]P concentration in the samples, which is above the linear calibration range. In order to determine the B[a]P concentration, the samples were additionally measured in a 100-fold dilution in DMSO. Prior to extraction with dichloromethane (DCM) (1:7.5 volume ratio), ethanol (EtOH) was added as a disperser (54) (1:2.5 volume ratio). After the addition of EtOH and DCM, the samples were vortexed for 1 min. Subsequently, the samples were centrifuged for 15 min at 4°C and 4,000 × g for better phase separation. The lower organic phase containing the analytes was separated, the extraction was repeated twice, and the combined organic extracts were concentrated to dryness in 1.5-ml Eppendorf tubes using the Concentrator Plus (Eppendorf, Hamburg, Germany) at 30°C. The residues were dissolved in 20 μl N,O-bis(trimethylsilyl)-trifluoracetamide (BSTFA) (99% BSTFA with 1% trimethylsilyl chloride) (15222-10X1ML-F; Sigma-Aldrich, St. Louis, MO, USA) as a derivatization agent in GC vials (2-ml crimp top with a 300-μl inlet; Agilent Technologies, Santa Clara, CA, USA) to accomplish silylation of functionalized B[a]P metabolites (Fig. S3A) at 60°C for 90 min and shaking at 120 rpm in a water bath. Subsequently, 1 μl of each sample was diluted in 99 μl fresh BSTFA for quantification of unmetabolized B[a]P via GC-MS.

(c) GC-MS measurements. One microliter of silylated sample mixture was injected in splitless mode into a gas chromatograph 6890 (Agilent) equipped with an HP-5MS capillary column (30-m length, 250-μm inner diameter, 0.25-μm film thickness, 10-m precolumn; Agilent) coupled to a 5975 mass spectrometric detector (Agilent). Electron impact (EI) ionization was conducted at 70 eV. The data acquisition was performed in combined single-ion monitoring (SIM)/full scan mode in order to achieve high sensitivity for target analytes while at the same time acquiring information on unknown metabolites which might be included in the samples. The column was operated in constant-flow mode (1 ml/min) with helium 5.0 as the carrier gas and an oven program ranging from 60°C (for 1 min) to 260°C (15°C/min) to 280°C (1°C/min) to 320°C (25°C/min and hold for 5 min). The temperature of the transfer line connecting to the mass spectrometer was set to 295°C. The injector was a cold injection system (Gerstel, Mülheim, Germany) operated with a temperature program starting at 45°C and ramping to 300°C at a rate of 12°C/s.

(d) Metabolite quantification. Metabolites were quantified using MassHunter quantitative analysis software 7.0 (Agilent Technologies, Santa Clara, CA, USA). Untreated skin models or cell culture media were used as blanks. A matrix calibration was performed using skin models or culture medium spiked with defined amounts of the B[a]P metabolites under consideration (Table 1). The calibration series was prepared by dilution of stock solutions in DMSO, so that the DMSO concentration in the final solution did not exceed 0.01%. The concentration range of the standards varied depending on their limit of detection (Table 2). Calibration curves were checked for linearity and used for quantification of the analytes (Fig. S3B). The B[a]P-diones contained in the samples are present in solution in a redox equilibrium with their respective dihydroxy-B[a]P counterparts (55). During the derivatization reaction, B[a]P-diones are reduced to their corresponding dihydroxy-B[a]Ps, which are silylated and subsequently analyzed by GC-MS. Therefore, the ratio between diones and dihydroxy analogs cannot be determined by this method (Fig. S3A). In bacterial metabolism, B[a]P-dihydrodiols can be converted to dihydroxy-B[a]P by dihydrodiol dehydrogenases (56, 57). However, since beside the B[a]P-7,8-dihydrodiol and the B[a]P-9,10-dihydrodiol no other metabolites with the corresponding mass spectra (m/z = 430, m/z = 340) were measured in our experiments, the presence of B[a]P-diones is much more likely here. Given a similar

TABLE 2 External standards[a]

Substance	RT (min)	Quantifier m/z	Qualifier m/z	Allocation to IS[b]	Calibration range (pmol)
B[*a*]P	26.7	252	253	1	2.5–2,500
3-OH-B[*a*]P	34.9	340	341	2	3.7–1,850
7-OH-B[*a*]P	34,6	340	341	2	3.7–370
9-OH-B[*a*]P	33.7	340	341	2	3.7–370
B[*a*]P-1,6-dione	41.8	428	429	3	8.9–1780
B[*a*]P-6,12-dione	38.5	428	429	3	8.9–1,780
B[*a*]P-7,8-dione	42.2	428	429	3	8.9–1,780
B[*a*]P-7,10-dione	33.7	428	429	3	8.9–1,780
B[*a*]P-7,8-dihydrodiol	35.4	430	340	4	17.6–1,760
B[*a*]P-9,10-dihydrodiol	28.3	430	340	4	17.6–1,760
B[*a*]P-7,8,9,10-tetrahydrotetrol	36.7	404	191	5	18.7–1,870

[a]External standards used for identification and quantification of the B[*a*]P metabolites using GC-MS.
[b]Designation corresponding to the IS listed in Table 1.

concentration of the B[*a*]P-7,8-dihydrodiol in the uncolonized controls and the colonized skin models, but a significantly higher concentration of B[*a*]P-7-8-dione in the latter, the presence of the dione can also be assumed.

BPDE-DNA adduct quantification. The BPDE-DNA adduct enzyme-linked immunosorbent assay (ELISA) (STA-357; Cell Biolabs, Inc., San Diego, CA, USA) was performed according to the manufacturer's instructions to compare BPDE-DNA adduct formation in colonized skin and control tissues. Initially, the DNA of the skin models was isolated with a TRIzol-based protocol using the TRIzol reagent (Thermo Scientific, Waltham, MA, USA) as described earlier (58). The DNA concentration was determined using the Qubit dsDNA HS assay kit (Q32851; Thermo Scientific, Waltham, MA, USA) in the Qubit 2.0 fluorometer (Thermo Scientific, Waltham, MA, USA). The absorbance was measured at 450 nm using a BioTek Synergy Neo2 spectrophotometer (BioTek Instruments, Winooski, VT, USA).

Statistical analysis. All experiments were performed with at least three biological replicates if not stated otherwise. Data are presented as means and standard deviations (SD). GraphPad Prism 8 (Statcon, Witzenhausen, Germany) was used for data analysis, illustration, and statistical data processing, with analyses of multiple groups by one-way analysis of variance (ANOVA) with Bonferroni's multiple-comparison test or ordinary two-way ANOVA being performed as appropriate. Data from the analytical investigations were normalized by dividing each value of the microbially colonized skin treated with B[*a*]P by the mean value of the respective control tissues treated with the same B[*a*]P stock solution but lacking skin bacteria and multiplying by 100 for the specification in percentages. For the evaluation of the Western blot data, the normalization was done by dividing the measurement of all different conditions by the value of the untreated control (no B[*a*]P and no bacteria) starting with the loading control (GAPDH) and then with the respective target. The normalization of data for immunofluorescence measurements was performed on the respective untreated control (no B[*a*]P and no bacteria), which was stained at the same time as the treatments. For the evaluation of the transcriptome data, the batch effect was included in the case of the B[*a*]P activating genes for comparability with our previous data (31). The batch effect considers the cultures treated with the same B[*a*]P stock solution. In general, a value of P of ≤ 0.05 was accepted as statistically significant.

Data availability. Raw and processed data files have been deposited in the Gene Expression Omnibus (GEO) data repository under accession number GSE171720.

SUPPLEMENTAL MATERIAL

Supplemental material is available online only.
DATA SET S1, JPG file, 2.5 MB.
FIG S1, JPG file, 0.5 MB.
FIG S2, JPG file, 0.2 MB.
FIG S3, JPG file, 0.9 MB.
FIG S4, JPG file, 1.1 MB.
FIG S5, JPG file, 0.3 MB.
FIG S6, JPG file, 1 MB.
FIG S7, JPG file, 1.1 MB.
FIG S8, JPG file, 0.8 MB.
TABLE S1, JPG file, 0.7 MB.

ACKNOWLEDGMENTS

REFERENCES

1. Korkina L. 2016. Metabolic and redox barriers in the skin exposed to drugs and xenobiotics. Expert Opin Drug Metab Toxicol 12:377–388. https://doi.org/10.1517/17425255.2016.1149569.

2. Ley RE, Peterson DA, Gordon JI. 2006. Ecological and evolutionary forces shaping microbial diversity in the human intestine. Cell 124:837–848. https://doi.org/10.1016/j.cell.2006.02.017.

3. Qin J, Li R, Raes J, Arumugam M, Burgdorf KS, Manichanh C, Nielsen T, Pons N, Levenez F, Yamada T, Mende DR, Li J, Xu J, Li S, Li D, Cao J, Wang B, Liang H, Zheng H, Xie Y, Tap J, Lepage P, Bertalan M, Batto JM, Hansen T, Le Paslier D, Linneberg A, Nielsen HB, Pelletier E, Renault P, Sicheritz-Ponten T, Turner K, Zhu H, Yu C, Li S, Jian M, Zhou Y, Li Y, Zhang X, Li S, Qin N, Yang H, Wang J, Brunak S, Dore J, Guarner F, Kristiansen K, Pedersen O, Parkhill J, Weissenbach J, MetaHIT Consortium, et al. 2010. A human gut microbial gene catalogue established by metagenomic sequencing. Nature 464:59–65. https://doi.org/10.1038/nature08821.

4. Sender R, Fuchs S, Milo R. 2016. Revised estimates for the number of human and bacteria cells in the body. PLoS Biol 14:e1002533. https://doi.org/10.1371/journal.pbio.1002533.

5. Scharschmidt TC, Fischbach MA. 2013. What lives on our skin: ecology, genomics and therapeutic opportunities of the skin microbiome. Drug Discov Today Dis Mech 10:e83–e89. https://doi.org/10.1016/j.ddmec.2012.12.003.

6. Chen YE, Fischbach MA, Belkaid Y. 2018. Skin microbiota-host interactions. Nature 553:427–436. https://doi.org/10.1038/nature25177.

7. Tralau T, Sowada J, Luch A. 2015. Insights on the human microbiome and its xenobiotic metabolism: what is known about its effects on human physiology? Expert Opin Drug Metab Toxicol 11:411–425. https://doi.org/10.1517/17425255.2015.990437.

8. Lange-Asschenfeldt B, Marenbach D, Lang C, Patzelt A, Ulrich M, Maltusch A, Terhorst D, Stockfleth E, Sterry W, Lademann J. 2011. Distribution of bacteria in the epidermal layers and hair follicles of the human skin. Skin Pharmacol Physiol 24:305–311. https://doi.org/10.1159/000328728.

9. Abdelsalam NA, Ramadan AT, ElRakaiby MT, Aziz RK. 2020. Toxicomicrobiomics: the human microbiome vs. pharmaceutical, dietary, and environmental xenobiotics. Front Pharmacol 11:390–390. https://doi.org/10.3389/fphar.2020.00390.

10. Martin AM, Sun EW, Rogers GB, Keating DJ. 2019. The influence of the gut microbiome on host metabolism through the regulation of gut hormone release. Front Physiol 10:428–428. https://doi.org/10.3389/fphys.2019.00428.

11. Koppel N, Maini Rekdal V, Balskus EP. 2017. Chemical transformation of xenobiotics by the human gut microbiota. Science (New York, NY) 356:eaag2770. https://doi.org/10.1126/science.aag2770.

12. Hayes CL, Dong J, Galipeau HJ, Jury J, McCarville J, Huang X, Wang X-Y, Naidoo A, Anbazhagan AN, Libertucci J, Sheridan C, Dudeja PK, Bowdish DME, Surette MG, Verdu EF. 2018. Commensal microbiota induces colonic barrier structure and functions that contribute to homeostasis. Sci Rep 8:14184. https://doi.org/10.1038/s41598-018-32366-6.

13. Hausmann C, Hertz-Kleptow D, Zoschke C, Wanjiku B, Wentzien-Odenthal A, Kerscher M, Schafer-Korting M. 2019. Reconstructed human epidermis predicts barrier-improving effects of Lactococcus lactis emulsion in humans. Skin Pharmacol Physiol 32:72–80. https://doi.org/10.1159/000495255.

14. Claus SP, Guillou H, Ellero-Simatos S. 2016. The gut microbiota: a major player in the toxicity of environmental pollutants? NPJ Biofilms Microbiomes 2:16003. https://doi.org/10.1038/npjbiofilms.2016.3.

15. Baklanov A, Hanninen O, Slordal LH, Kukkonen J, Bjergene N, Fay B, Finardi S, Hoe SC, Jantunen M, Karppinen A, Rasmussen A, Skouloudis A, Sokhi RS, Sorensen JH, Odegaard V. 2007. Integrated systems for forecasting urban meteorology, air pollution and population exposure. Atmos Chem Phys 7:855–874. https://doi.org/10.5194/acp-7-855-2007.

16. Manzetti S. 2013. Polycyclic aromatic hydrocarbons in the environment: environmental fate and transformation. Polycyclic Aromatic Compounds 33:311–330. https://doi.org/10.1080/10406638.2013.781042.

17. Geier MC, Chlebowski AC, Truong L, Massey Simonich SL, Anderson KA, Tanguay RL. 2018. Comparative developmental toxicity of a comprehensive suite of polycyclic aromatic hydrocarbons. Arch Toxicol 92:571–586. https://doi.org/10.1007/s00204-017-2068-9.

18. Bamforth SM, Singleton I. 2005. Bioremediation of polycyclic aromatic hydrocarbons: current knowledge and future directions. J Chem Technol Biotechnol 80:723–736. https://doi.org/10.1002/jctb.1276.

19. Luch A, Baird WM. 2005. Metabolic activation and eetoxification of polycyclic aromatic hydrocarbons, p 19–96. In Luch A (ed), The carcinogenic effects of polycyclic aromatic hydrocarbons. Imperial College Press, London, United Kingdom.

20. Baird WM, Hooven LA, Mahadevan B. 2005. Carcinogenic polycyclic aromatic hydrocarbon-DNA adducts and mechanism of action. Environ Mol Mutagen 45:106–114. https://doi.org/10.1002/em.20095.

21. Jernstrom B, Graslund A. 1994. Covalent binding of benzo[a]pyrene 7,8-dihydrodiol 9,10-epoxides to DNA: molecular structures, induced mutations and biological consequences. Biophys Chem 49:185–199. https://doi.org/10.1016/0301-4622(93)E0087-L.

22. Uno S, Dalton TP, Derkenne S, Curran CP, Miller ML, Shertzer HG, Nebert DW. 2004. Oral exposure to benzo[a]pyrene in the mouse: detoxication by inducible cytochrome P450 is more important than metabolic activation. Mol Pharmacol 65:1225–1237. https://doi.org/10.1124/mol.65.5.1225.

23. Marks R. 2004. The stratum corneum barrier: the final frontier. J Nutr 134:2017S–2021S. https://doi.org/10.1093/jn/134.8.2017S.

24. Marczynski B, Pesch B, Wilhelm M, Rossbach B, Preuss R, Hahn JU, Rabstein S, Raulf-Heimsoth M, Seidel A, Rihs HP, Adams A, Scherenberg M, Erkes A, Engelhardt B, Straif K, Käfferlein HU, Angerer J, Brüning T. 2009. Occupational exposure to polycyclic aromatic hydrocarbons and DNA damage by industry: a nationwide study in Germany. Arch Toxicol 83:947–957. https://doi.org/10.1007/s00204-009-0444-9.

25. VanRooij JG, De Roos JH, Bodelier-Bade MM, Jongeneelen FJ. 1993. Absorption of polycyclic aromatic hydrocarbons through human skin: differences between anatomical sites and individuals. J Toxicol Environ Health 38:355–368. https://doi.org/10.1080/15287399309531724.

26. Sowada J, Schmalenberger A, Ebner I, Luch A, Tralau T. 2014. Degradation of benzo[a]pyrene by bacterial isolates from human skin. FEMS Microbiol Ecol 88:129–139. https://doi.org/10.1111/1574-6941.12276.

27. Sowada J, Lemoine L, Schon K, Hutzler C, Luch A, Tralau T. 2017. Toxification of polycyclic aromatic hydrocarbons by commensal bacteria from human skin. Arch Toxicol 91:2331–2341. https://doi.org/10.1007/s00204-017-1964-3.

28. Toda T, Saito N, Ikarashi N, Ito K, Yamamoto M, Ishige A, Watanabe K, Sugiyama K. 2009. Intestinal flora induces the expression of Cyp3a in the mouse liver. Xenobiotica 39:323–334. https://doi.org/10.1080/00498250802651984.

29. Meinl W, Sczesny S, Brigelius-Flohe R, Blaut M, Glatt H. 2009. Impact of gut microbiota on intestinal and hepatic levels of phase 2 xenobiotic-metabolizing enzymes in the rat. Drug Metab Dispos 37:1179–1186. https://doi.org/10.1124/dmd.108.025916.

30. Defois C, Ratel J, Denis S, Batut B, Beugnot R, Peyretaillade E, Engel E, Peyret P. 2017. Environmental pollutant benzo[a]pyrene impacts the volatile metabolome and transcriptome of the human gut microbiota. Front Microbiol 8:1562. https://doi.org/10.3389/fmicb.2017.01562.

31. Lemoine L, Dieckmann R, Al Dahouk S, Vincze S, Luch A, Tralau T. 2020. Microbially competent 3D skin: a test system that reveals insight into host-microbe interactions and their potential toxicological impact. Arch Toxicol 94:3487–3502. https://doi.org/10.1007/s00204-020-02841-z.

32. Collins SL, Patterson AD. 2020. The gut microbiome: an orchestrator of xenobiotic metabolism. Acta Pharm Sin B 10:19–32. https://doi.org/10.1016/j.apsb.2019.12.001.

33. Tralau T, Luch A. 2017. The human microbiome, from Achilles armour to Nessus' shirt. Arch Toxicol 91:2699–2701. https://doi.org/10.1007/s00204-017-1951-8.

34. Licht TR, Bahl MI. 2019. Impact of the gut microbiota on chemical risk assessment. Curr Opin Toxicol 15:109–113. https://doi.org/10.1016/j.cotox.2018.09.004.

35. Riebeling C, Luch A, Tralau T. 2018. Skin toxicology and 3Rs—current challenges for public health protection. Exp Dermatol 27:526–536. https://doi.org/10.1111/exd.13536.

36. Juhasz AL, Naidu R. 2000. Bioremediation of high molecular weight polycyclic aromatic hydrocarbons: a review of the microbial degradation of benzo[a]pyrene. Int Biodeterior Biodegrad 45:57–88. https://doi.org/10.1016/S0964-8305(00)00052-4.

37. Brinkmann J, Stolpmann K, Trappe S, Otter T, Genkinger D, Bock U, Liebsch M, Henkler F, Hutzler C, Luch A. 2013. Metabolically competent human skin models: activation and genotoxicity of benzo[a]pyrene. Toxicol Sci 131:351–359. https://doi.org/10.1093/toxsci/kfs316.

38. Chu I, Dick D, Bronaugh R, Tryphonas L. 1996. Skin reservoir formation and bioavailability of dermally administered chemicals in hairless guinea pigs. Food Chem Toxicol 34:267–276. https://doi.org/10.1016/0278-6915(95)00112-3.

39. Bourgart E, Barbeau D, Marques M, von Koschembahr A, Béal D, Persoons R, Leccia M-T, Douki T, Maitre A. 2019. A realistic human skin model to study benzo[a]pyrene cutaneous absorption in order to determine the most relevant biomarker for carcinogenic exposure. Arch Toxicol 93:81–93. https://doi.org/10.1007/s00204-018-2329-2.

40. Meisel JS, Sfyroera G, Bartow-McKenney C, Gimblet C, Bugayev J, Horwinski J, Kim B, Brestoff JR, Tyldsley AS, Zheng Q, Hodkinson BP, Artis D, Grice EA. 2018. Commensal microbiota modulate gene expression in the skin. Microbiome 6:20–20. https://doi.org/10.1186/s40168-018-0404-9.

41. Toulza E, Mattiuzzo NR, Galliano M-F, Jonca N, Dossat C, Jacob D, de Daruvar A, Wincker P, Serre G, Guerrin M. 2007. Large-scale identification of human genes implicated in epidermal barrier function. Genome Biol 8:R107. https://doi.org/10.1186/gb-2007-8-6-r107.

42. Fischer H, Stichenwirth M, Dockal M, Ghannadan M, Buchberger M, Bach J, Kapetanopoulos A, Declercq W, Tschachler E, Eckhart L. 2004. Stratum corneum-derived caspase-14 is catalytically active. FEBS Lett 577:446–450. https://doi.org/10.1016/j.febslet.2004.10.046.

43. Landemaine L, Cenizo V, Lemaire G, Portes P. 2018. 961 Colonization of a 3D skin model with a complete microbiota is more beneficial to the skin barrier than with Staphylococcus epidermidis alone. J Investig Dermatol 138:S163. https://doi.org/10.1016/j.jid.2018.03.973.

44. Loomis KH, Wu SK, Ernlund A, Zudock K, Reno A, Blount K, Karig DK. 2021. A mixed community of skin microbiome representatives influences cutaneous processes more than individual members. Microbiome 9:22. https://doi.org/10.1186/s40168-020-00963-1.

45. Joensen UN, Jørgensen N, Meldgaard M, Frederiksen H, Andersson AM, Menné T, Johansen JD, Carlsen BC, Stender S, Szecsi PB, Skakkebæk NE, Rajpert-De Meyts E, Thyssen JP. 2014. Associations of filaggrin gene loss-of-function variants with urinary phthalate metabolites and testicular function in young Danish Men. Environ Health Perspect 122:345–350. https://doi.org/10.1289/ehp.1306720.

46. Sevilla LM, Nachat R, Groot KR, Klement JF, Uitto J, Djian P, Määttä A, Watt FM. 2007. Mice deficient in involucrin, envoplakin, and periplakin have a defective epidermal barrier. J Cell Biol 179:1599–1612. https://doi.org/10.1083/jcb.200706187.

47. Jensen JM, Schütze S, Neumann C, Proksch E. 2000. Impaired cutaneous permeability barrier function, skin hydration, and sphingomyelinase activity in keratin 10 deficient mice. J Invest Dermatol 115:708–713. https://doi.org/10.1046/j.1523-1747.2000.00103.x.

48. Ulluwishewa D, Anderson RC, McNabb WC, Moughan PJ, Wells JM, Roy NC. 2011. Regulation of tight junction permeability by intestinal bacteria and dietary components. J Nutr 141:769–776. https://doi.org/10.3945/jn.110.135657.

49. Jacques C, Perdu E, Duplan H, Jamin EL, Canlet C, Debrauwer L, Cravedi JP, Mavon A, Zalko D. 2010. Disposition and biotransformation of 14C-benzo(a)pyrene in a pig ear skin model: ex vivo and in vitro approaches. Toxicol Lett 199:22–33. https://doi.org/10.1016/j.toxlet.2010.08.001.

50. Jaiswal SK, Agarwal SM, Thodum P, Sharma VK. 2021. SkinBug: an artificial intelligence approach to predict human skin microbiome-mediated metabolism of biotics and xenobiotics. iScience 24:101925. https://doi.org/10.1016/j.isci.2020.101925.

51. Chomczynski P, Sacchi N. 1987. Single-step method of RNA isolation by acid guanidinium thiocyanate-phenol-chloroform extraction. Anal Biochem 162:156–159. https://doi.org/10.1006/abio.1987.9999.

52. Hering H, Zoschke C, Kühn M, Gadicherla AK, Weindl G, Luch A, Schreiver I. 2020. TatS: a novel in vitro tattooed human skin model for improved pigment toxicology research. Arch Toxicol 94:2423–2434. https://doi.org/10.1007/s00204-020-02825-z.

53. de Bruin OM, Birnboim HC. 2016. A method for assessing efficiency of bacterial cell disruption and DNA release. BMC Microbiol 16:197. https://doi.org/10.1186/s12866-016-0815-3.

54. Sadeghi R, Kobarfard F, Yazdanpanah H, Eslamizad S, Bayat M. 2016. Validation of an analytical method for determination of 13 priority polycyclic aromatic hydrocarbons in mineral water using dispersive liquid-liquid microextraction and GC-MS. Iran J Pharm Res 15:157–168.

55. Song Y, Buettner GR. 2010. Thermodynamic and kinetic considerations for the reaction of semiquinone radicals to form superoxide and hydrogen peroxide. Free Radic Biol Med 49:919–962. https://doi.org/10.1016/j.freeradbiomed.2010.05.009.

56. Ostrem Loss EM, Lee M-K, Wu M-Y, Martien J, Chen W, Amador-Noguez D, Jefcoate C, Remucal C, Jung S, Kim S-C, Yu J-H. 2019. Cytochrome P450 monooxygenase-mediated metabolic utilization of benzo[a]pyrene by Aspergillus species. mBio 10:e00558-19. https://doi.org/10.1128/mBio.00558-19.

57. Moody JD, Freeman JP, Fu PP, Cerniglia CE. 2004. Degradation of benzo[a]pyrene by Mycobacterium vanbaalenii PYR-1. Appl Environ Microbiol 70:340–345. https://doi.org/10.1128/AEM.70.1.340-345.2004.

58. Chomczynski P. 1993. A reagent for the single-step simultaneous isolation of RNA, DNA and proteins from cell and tissue samples. Biotechniques 15:532–534. 536-7.